Oil & Natural Gas Technology

DOE Award No.: DE-FE0013889

Quarterly Research Performance Progress Report (Period ending 06/30/2016)

THCM Coupled Model For Hydrate-Bearing Sediments: Data Analysis and Design of New Field Experiments (Marine and Permafrost Settings)

Project Period (10/1/2013 to 09/30/2016)

Submitted by:

Marcelo Sanchez Project PI

Texas A&M University
DUNS #: 847205572
College Station, TX
979-862-6604
msanchez@civil.tamu

Prepared for:
United States Department of Energy
National Energy Technology Laboratory
Submission date: 08/04/2016

Office of Fossil Energy

DISCLAIMER

ACCOMPLISHMENTS

The experimental study of hydrate bearing sediments has been hindered by the very low solubility of methane in water (lab testing), and inherent sampling difficulties associated with depressurization and thermal changes during core extraction. This situation has prompted more decisive developments in numerical modeling in order to advance the current understanding of hydrate bearing sediments, and to investigate/optimize production strategies and implications. The goals of this research is to addresses the complex thermo-hydro-chemo-mechanical THCM coupled phenomena in hydrate-bearing sediments, using a truly coupled numerical model that incorporates sound and proven constitutive relations, satisfies fundamental conservation principles. This tool will allow us to better analyze available data and to further enhance our understanding of hydrate bearing sediments in view of future field experiments and the development of production technology.

ACCOMPLISHED

The main accomplishments for this period address Tasks 5 and 7 of the original research plan, and include:

- Update of constitutive equations.
- Update of THCM-Hydrate.
- Numerical analyses.
- Incorporation of additional THCM-Hydrate code modifications.
- Production Optimization of Future Field Studies.

Training

The training of the two PhD students working in this project has continued during this period. Mr. Xuerui (Gary) Gai was hired at the start of the project and his activities have been related to the use of code "THCM-Hydrate"; which is the numerical tool under development in this project. His research has focused on the mechanical modeling of Hydrate Bearing Sediments (HBS). Mr. Mehdi Teymouri was hired at the beginning of the second year of the project. His research has focused on modeling numerical and analytical methods in hydrates research. He is also working in sand production when producing gas from methane hydrate reservoirs. Both students have progressed positively with their coursework at their respective universities.

Literature review

The literature review (Task 2) was completed in a previous period.

Update of THCM-Hydrate

The update of the constitutive laws for hydrate-bearing marine sediments and HBS in the permafrost (i.e. Task 3) was completed in a previous period.

Close-form analytical solutions

The review on the main governing evolution laws, parameters, dimensionless ratios and simplifying assumptions for HBS dissociation (i.e. Task 4) was completed in previous periods.

Numerical analyses

The numerical analyses related to HBS sediments have been continued in this period. In page 6 a study related to water retention behavior in heterogeneous sediments during gas injection experiments is presented. In page 15 a study related to the mechanical behavior of HBS is discussed.

Plan - Next reporting period

We will advance analytical and numerical fronts to enhance our code to solve coupled THCM problems involving with HBS, with renewed emphasis on simulating the natural processes under *in-situ* conditions and gas production.

.

Milestones for each budget period of the project are tabulated next. These milestones are selected to show progression towards project goals.

	Milestone Title Planned Date and Verification Method	Actual Completion Date	Comments
Title Related Task / Subtasks Planned Date Verification method	Complete literature review 2.0 / 2.a March 2014 Report	March 2014	Completed
Title Related Task / Subtasks Planned Date Verification method	Complete updated Constitutive Equations 2.0 / 2.b & 2.c June 2014 Report (with preliminary validation data)	July 2014	Completed
Title Related Task / Subtasks Planned Date Verification method	Validate new THCM constitutive equations 3.0 / 3.a, 3.b & 3.c September 2014 Report (with first comparisons between experimental and numerical results)	September 2014	Completed
Title Related Task / Subtasks Planned Date Verification method	Complete close-form analytical solutions 4.0 / 4.a & 4.b February 2015 Report (with analytical data)	February 2015	Completed
Title Related Task / Subtasks Planned Date Verification method	Complete numerical analyses 5.0 / 5.a, 5.b & 5.c July 2015 Report (with analytical and numerical data)	July 2016	Progressing as planned
Title Related Task / Subtasks Planned Date Verification method	Complete THCM-Hydrate code modifications 6.0 / 6.a June 2015 Report (with numerical data)	June 2016	Completed
Title Related Task / Subtasks Planned Date Verification method	Complete production optimization 7.0 / 7.a, 7.b, 7.c, 7.d & 7.e September 2015 Report (with numerical data)	September 2016	Progressing as planned

CAPILLARY PRESSURE - PARTIAL SATURATION CURVES FOR SEDIMENTS WITH NON-UNIFORM DISTRIBUTION OF HYDRAULIC PROPERTIES

1. INTRODUCTION

The capillary pressure-saturation relationship, also known as soil-water characteristic curve or Soil Water Retention Curve (SWRC), defines the ability of a sediment to retain liquid at different capillary pressures (i.e. where the capillary pressure is defined as the difference between the gas and the liquid pressures: $P_c=P_g-P_\ell$.). The SWRC is generally expressed in terms of capillary pressure and liquid phase saturation (also known as degree of liquid saturation, S_l, given by the ratio between the volume of liquid and volume of voids). The SWRC plays a central role in the modeling of problems involving gas Hydrate Bearing Sediments HBS (e.g. Rutqvist and Moridis, 2009; Klar et al., 2010; Kimoto et al., 2007).

In this work, numerical simulations were conducted to study the water retention properties of sediments with randomly distributed properties under gas injection conditions. Two phase flow problems were solved assuming a rigid solid skeleton. Case studies based on different random porosity fields were considered in this research. It has been observed that the distribution of properties in HBS is quite heterogeneous, furthermore, a non-uniform porosity distribution in sediments may be anticipated which can be induced by the hydrate dissociation. Therefore, the study of the effect of non-uniform porosity fields on sediments retention capacity can be relevant to forecast gas production from HBS.

Advective fluxes are computed using a generalized Darcy's law, expressed as (e.g. Gens et al., 1998):

$$\mathbf{q}_\alpha = -\mathbf{K}_\alpha \left(\nabla P_\alpha - \rho_\alpha \mathbf{g}\right); \qquad \alpha = l, g \tag{1}$$

where P_α is the phase pressure. $\mathbf{K}_\alpha$ is the permeability tensor of α phase and $\mathbf{g}$ is the gravity vector.

The permeability tensor is evaluated according to:

$$\mathbf{K}_\alpha = \mathbf{k}\frac{k_{r\alpha}}{\mu_\alpha}; \qquad \alpha = l, g \tag{2}$$

where $\mathbf{k}$ is the intrinsic permeability tensor, μ_α is the dynamic viscosity of the α phase and $k_{r\alpha}$ is the phase relative permeability.

The dependence of intrinsic permeability on porosity was based on Kozeny's law:

$$\mathbf{k} = k_0 \frac{\phi^3}{(1-\phi)^2} \frac{(1-\phi_0)^2}{\phi_0^3} \mathbf{I} \tag{3}$$

where k_0 is the reference saturated permeability at the reference porosity ϕ_0.

The well-known power law was adopted to describe the dependence of liquid permeability on degree of saturation:

$$k_{rl} = S_l^n \tag{4}$$

A value of n=1 was assumed for the simulations. It was also considered that the relative permeability of the gas phase is obtained as: $k_{rg}=1-k_{rl}$.

A van Genuchten model (van Genuchten, 1980) expressed in terms of the effective liquid saturation (S^*_l) was adopted in the simulations, as follows:

$$S_\ell^* = \frac{S_\ell}{S_\ell + S_g} = \left[1 + \left(\frac{P_c}{P_o}\right)^{\frac{1}{1-\lambda}}\right]^{-\lambda} \tag{5}$$

where S_g is the gas saturation, P_o and λ are model parameters. P_o is also known as the 'air entry value parameter' and it is related to the breakthrough gas pressure necessary to start the desaturation of the material. This parameter can be associated with specimen porosity (i.e. Rodriguez et al., 2007; Le et al., 2013). The parameter λ is related to the rate at which desaturation takes place in sediments and it can be associated with the specimen grains size distribution.

2. CASE STUDY

The cases adopted in this study were based on the combination of two basic materials: 'A' and 'B'. The porosity values for material A and B were assumed equal to 0.05 and 0.3, respectively. The materials A and B were randomly distributed and mixed in different percentages to generate three different synthetic specimens, two additional reference cases with uniform properties equal to materials A and B were also studied. The five analyzed cases are:

- Case 1: material A 50%, material B 50% (volume fraction).
- Case 2: material A 75%, material B 25% (volume fraction).
- Case 3: material A 25%, material B 75% .
- Case 4: 100 % material A

- Case 5: 100 % material B

It was assumed that the permeability of the material depends on porosity through Kozeny's law (i.e. Eq. 3). As in others previous works (e.g. Rodriguez et al., 2007 and Le et al., 2012), it has been assumed that the air entry value (P_o, Eq. 5) depends on the porosity. Based on the correlation suggested by Le et al. (2012) it was assumed that P_o=0.1694 MPa for material A and P_o=0.01391MPa for material B. Therefore, in the Cases 1 to 3 the permeability and SWRC properties are randomly distributed because of their dependence with the porosity field

Figure 1a presents the geometry adopted for the analyses for a typical case. All the cases were analyzed following the same protocol. The specimens were initially fully saturated, with a capillary pressure P_c=0.0 MPa (i.e. P_l= P_g=0.1 MPa). Then, to induce the fluid flow along the sample, the gas pressure was increased in the top face by steps. No fluid flow was allowed through the lateral faces of the specimen. Per each step, the increment of gas pressure was increased linearly during one day and then it was kept constant until steady state conditions were achieved (generally 7 days). Figure 1b a shows a typical result in terms of degree of saturation. Figure 2 presents the protocol adopted to increase the gas pressure in the synthetic tests.

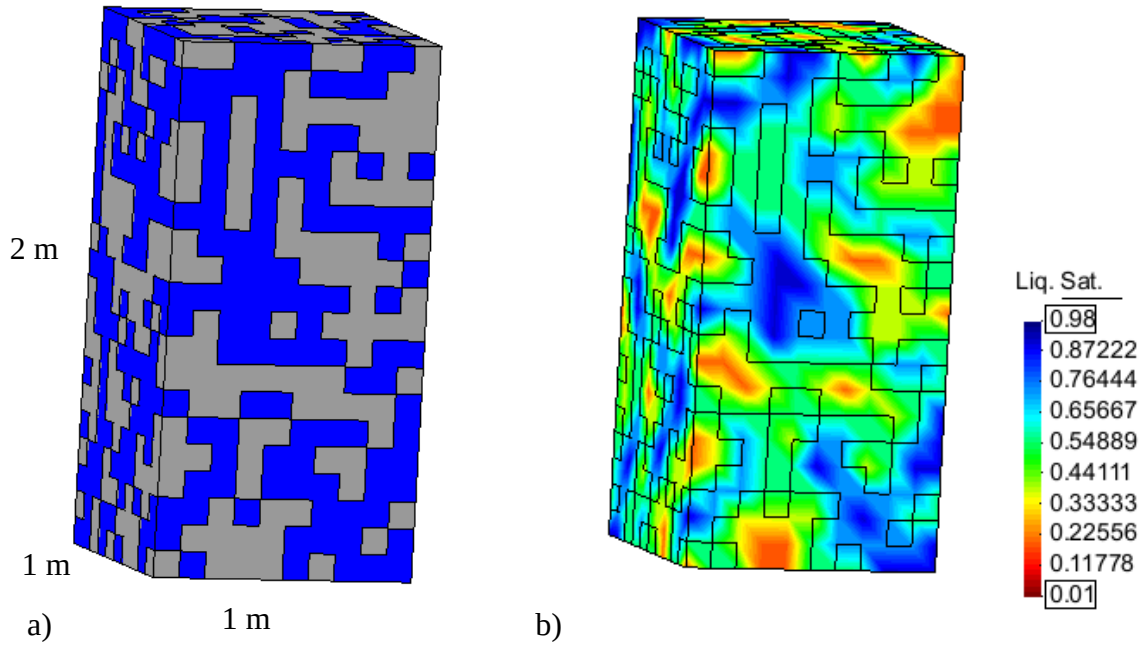

Figure 1. a) Geometry of a typical case, b) typical results in terms of degree of saturation.

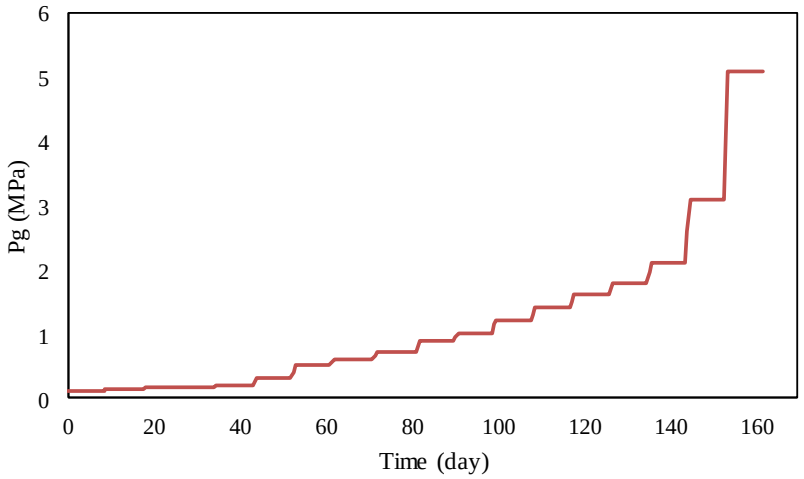

Figure 2. Evolution of applied gas pressure on top of the sample

3. MODELING RESULTS

Contours of liquid saturation at selected times (i.e. days 1, 8, 15, 40, 64, 96, 136 and 167) for Cases 1, 2 and 3 are shown in Figures 3, 4 and 5, respectively. It can be observed that the gas phase was gradually percolating through the sample during the test. A heterogeneous distribution of degree of liquid saturation at different stages is evident, associated with the random distribution of material properties. For the Cases 4 and 5 (i.e. the ones with uniform distributions of material properties), homogenous distributions of degree of saturation were obtained (as expected) at the different injection stages.

Figure 6 shows the SWRCs obtained from the simulations of the different cases considered in this study. The analytical solutions for the homogenous Cases A and B is also presented. A perfect agreement between analytical and numerical results can be observed for those two cases (i.e. Cases 4 & 5). For Case 1, the SWRC lies in between the curves of materials A & B. The SWRCs for Cases 2 and 3 are also in between the SWRCs for Cases 1 & 5 and 1 & 4, respectively.

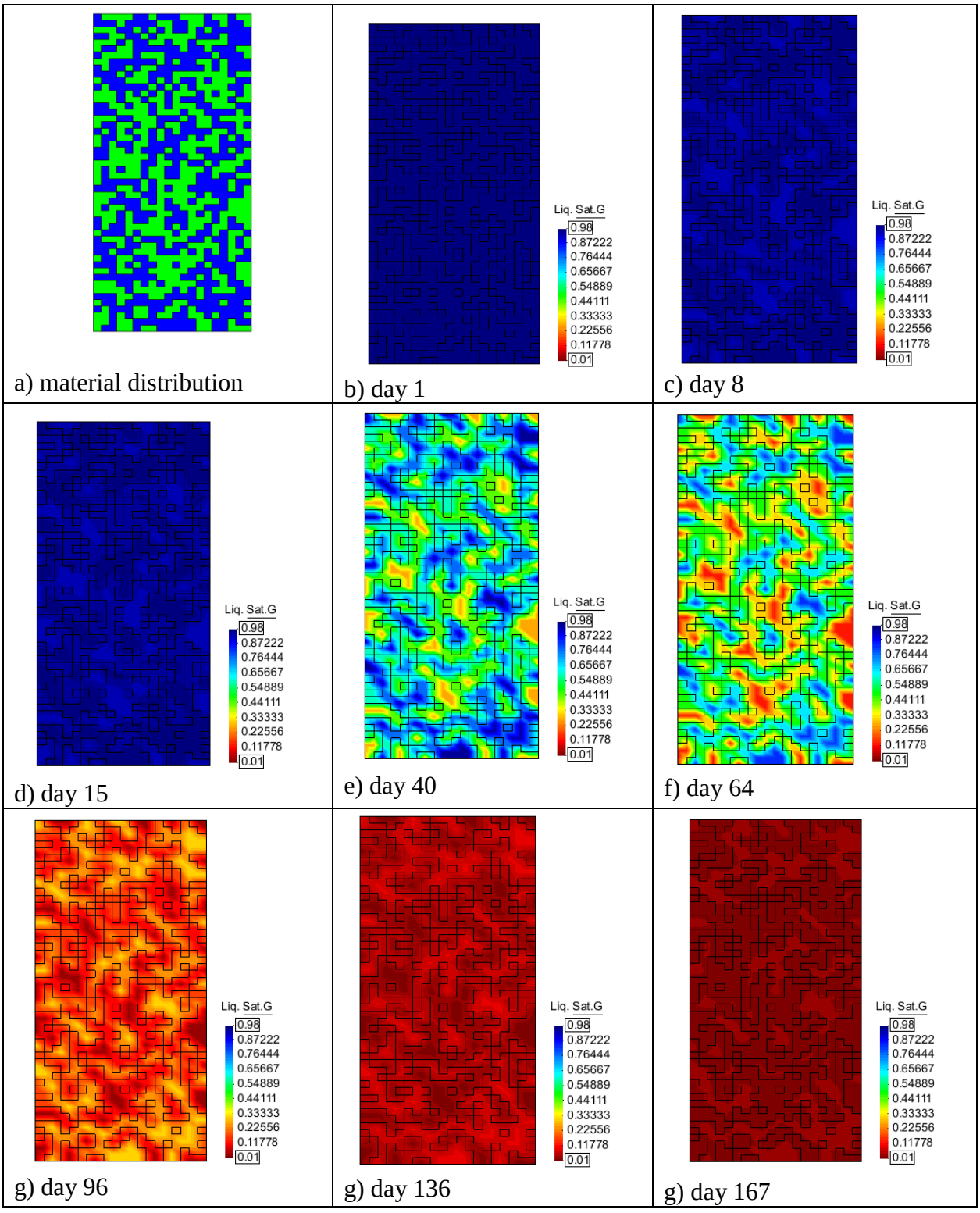

Figure 3. Time evolution of liquid saturation for Case 1

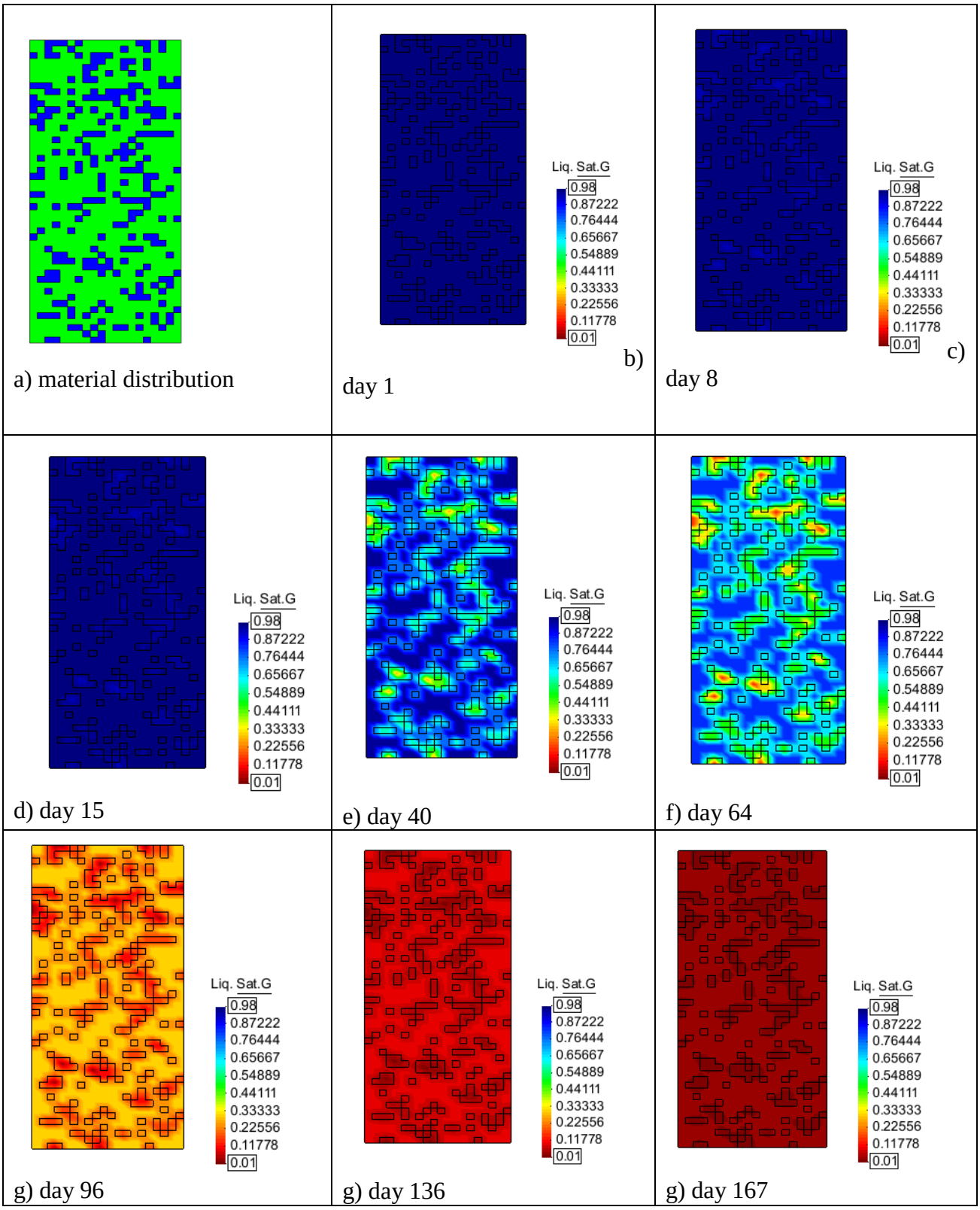

Figure 4. Time evolution of liquid saturation for Case 2

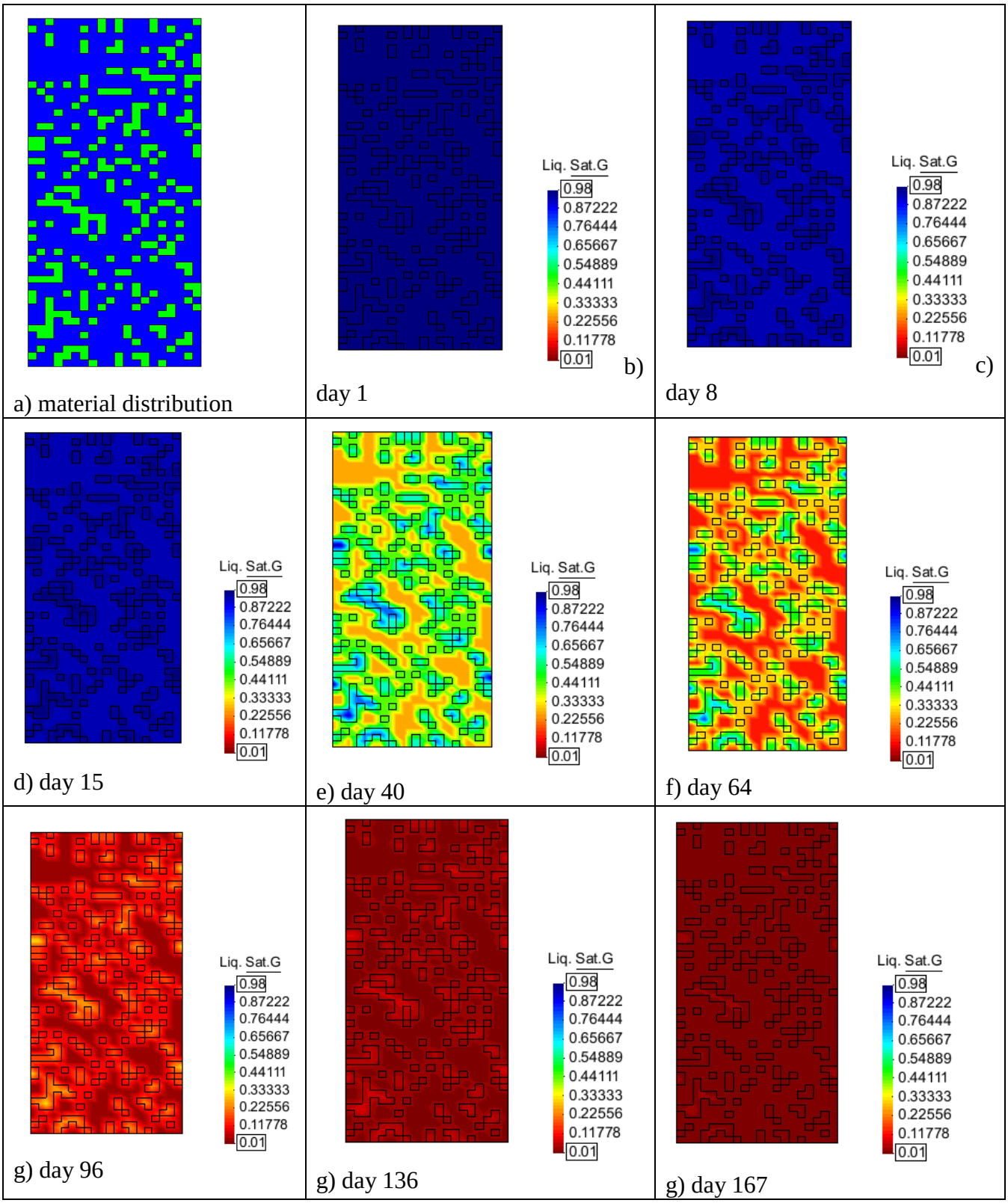

Figure 5. Time evolution of liquid saturation for Case 3

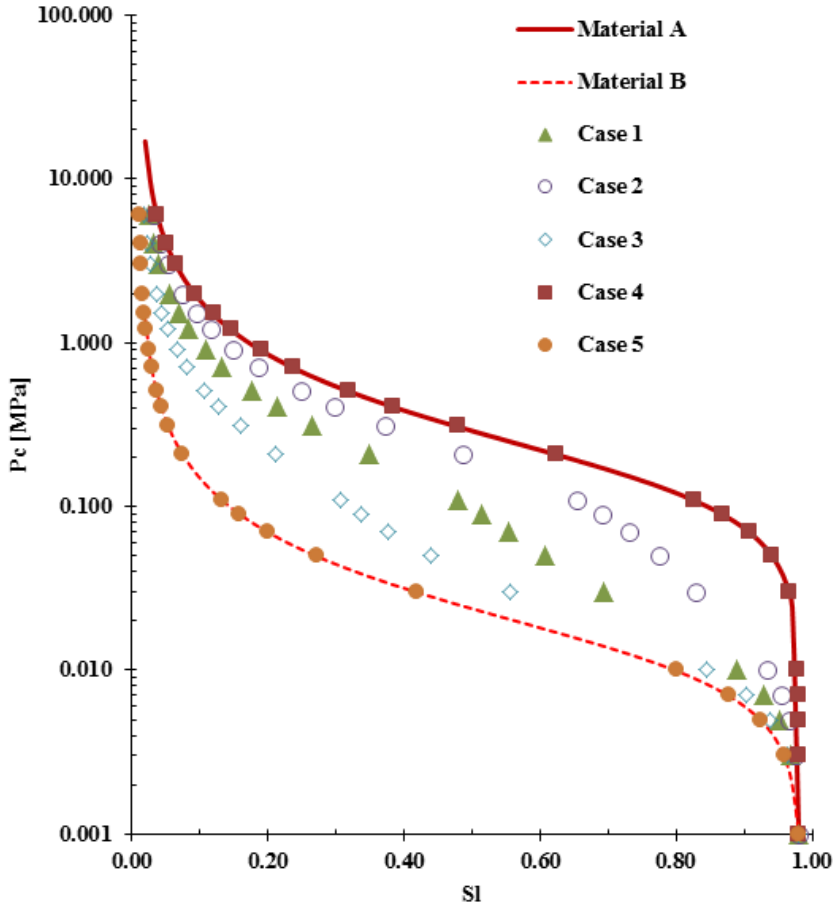

Figure 6. Capillary pressure – saturation curves for the different analyzed Cases.

4. FINAL REMARKS

Heterogeneous distribution of material properties in HBS is anticipated. Furthermore, non-uniform distribution of porosity during hydrate dissociation is expected. Therefore, understanding the impact of non-uniform porosity fields on water retention capacity of sediments can be relevant to forecast gas production from HBS. Numerical analyses simulating gas injection tests involving synthetic samples with non-uniform and uniform distributions of porosity values were conducted to study the effect of heterogeneity on water retention behavior of sediments. It was assumed that the hydraulic parameters related to the SWRC and hydraulic conductivity law were dependent on porosity. Non-uniform distributions of phase saturations were obtained.

REFERENCES

Gens A, Garcia Molina A, Olivella S, Alonso EE, Huertas, F. (1998). Analysis of a full scale in-situ test simulating repository conditions. *Int. Jnl. Numer. Anal. Meth. Geomech*.; **22**: 515-548.

Kimoto, S., Oka, F., Fushita, T., & Fujiwaki, M. (2007). A chemo-thermo-mechanically coupled numerical simulation of the subsurface ground deformations due to methane hydrate dissocia-tion. *Computers and Geotechnics*, 34(4), 216-228.

Klar, A., Soga, K., & Ng, M. Y. A. (2010). Coupled deformation–flow analysis for methane hydrate extraction. *Geotechnique*, 60(10), 765-776

Le, T. M. H., Gallipoli, D., Sanchez, M., & Wheeler, S. J. (2012). Stochastic analysis of unsaturated seepage through randomly heterogeneous earth embankments. *International Journal for Numerical and Analytical Methods in Geomechanics*, 36(8), 1056-1076.

Rodríguez R, Sánchez M, Lloret A, Ledesma A. (2007). Experimental and numerical analysis of a mining waste desiccation. Canadian Geotechnical Journal; 44:644-658

Rutqvist, J., & Moridis, G. J. (2009). Numerical studies on the geomechanical stability of hydrate-bearing sediments. *Spe Journal*, 14(02), 267-282.

van Genuchten, M. T. (1980). A closed-form equa-tion for predicting the hydraulic conductivity of unsaturated soils. *Soil Science Society of America Journal*, 44(5), 892-898.

HIIS-MH MODEL – A PARAMETRIC STUDY

1. INTRODUCTION

The constitutive mechanical model for hydrate bearing sediments HIIS-MH was presented in Sanchez (2015). In this section a study exploring the effect of some key parameters on the model performance is conducted. The Hierarchical Single Surface (HISS) framework proposed by Desai et al. (1986) was adopted in an effort to provide a more general and versatile constitutive model for HBS. Also many of the concepts suggested by Uchida et al. (2012) to deal with specific features of hydrate-bearing soils were incorporated into this model. Several applications of HISS-MH model were analyzed before and in this section, the parameter selections related with these applications are introduced.

The full mathematical framework related to this model was introduced in Sanchez (2015) For the sake of completeness, the main model equations are presented here only. More detail about the model and its application can be found elsewhere (i.e. Sanchez, 2015).

The HISS-MH model involves a single and continuous yield surface, which can have different shapes depending on the adopted parameters. The HISS yield surface (F) is expressed incorporating sub- loading concepts and as:

$$F = \frac{a}{M^2} q^2 - \gamma 3^2 p'^2 + \gamma 3^2 p'^n \left[\mathrm{R}(p_c + p_d) \right]^{2-n} \tag{1}$$

where a and γ are constants; n is the parameter related to the transition from compressive to dilative volume change; p' and q are the mean effective and deviatoric stresses, respectively; M is the slope of critical line in the q-p' space; p_c is the effective pre-consolidation pressure; hardening variable (p_d); and R is related to subloading concepts through the following evolution law:

$$\mathrm{dR} = -\eta \ln \mathrm{R} \left| d\boldsymbol{\varepsilon}^p \right| \tag{2}$$

where $|\mathrm{d}\varepsilon^{\mathrm{p}}|$ is the norm of the (total) plastic strain vector and η is a sub-loading parameter associated with any plastic deformations that may develop inside initial yield surface.

The hardening variable (p_d) is expressed as:

$$p_d = \alpha(\chi\, S_H)^{\beta} \tag{3}$$

where p_d controls the increase of the sediment strength associated with the presence of hydrates; α and β are constants that describe the degree of hydrate contribution to the hardening law; χ is a damage factor that varies between 1 (maximum bonding effect provided by the hydrate) and 0 (no bonding effect). This degradation effect is incorporated by defining the following evolution law for χ:

$$d\chi = -\mu\, \chi\, d\varepsilon_q^p \tag{4}$$

where μ is a parameter that defines the rate of mechanical damage and $d\varepsilon^p{}_q$ is the plastic deviatoric strain.

An advantage of the HISS is its flexibility to adapt the shape of the yield surface to the particular conditions of the soil under investigation by modifying three parameters (a, γ and n). Note that the MCC yield surface corresponds to a particular case of this model.

As in other typical soil mechanic models, the increment of the elastic volumetric strains depend directly on the increment of the mean effective stress (p') through the stress-dependent elastic soil bulk modulus K':

$$K' = \frac{v}{\kappa} p' \tag{5}$$

where v is the specific volume (v =1+e, where e is the void ratio); and κ is the slope of the unloading/reloading line in the *e-log(p)'* space.

Deviatoric elastic strains and stresses relate through the shear modulus (G_s). It is also assumed that the hardening law is isotropic and depends on the plastic volumetric strains (ε_v^p) through:

$$\frac{dp_c}{p_c} = \frac{v}{\lambda - \kappa} d\varepsilon_v^p \tag{6}$$

where λ is the slope of the normal compression line in the *e-log(p)'* space. For the sake of the simplicity, an associated flow rule is assumed (i.e. F coincide with the plastic potential G).

The first step is to determine the model parameters associated with the 'hydrate-free' sediment. An elastoplastic critical state model was adopted in this work, therefore the determination of the model parameters (i.e. κ, λ, G, p_o, and M) follows the typical procedure used in soils mechanics for this type of model. The only difference here is that the HISS yield surface and plastic

potential were adopted. Considering that the modified cam-clay mode (MCCM) is a particular case of the HISS model, the procedure followed hereafter was to determine first the parameters associated with MCCM. If the MCCM response is satisfactory, there is no need to change the model and the MCCM is adopted to describe the behavior of the pure sediment. However, if the MCCM performance is not optimal or acceptable, advantage of the HISS flexibility was taken to adapt the shape of the yield surface or plastic potential to enhance the model performance. An example of how this can be done is presented later in this section.

The parameters related to the effect of hydrates on sediment behavior are a bit more difficult to determine. The model incorporates evolution laws capable of considering in the (macroscopic) modeling, aspects related to the HBS structure (as e.g. S_H and pore habit). These parameters are associated with the increase of preconsolidation pressure and sediment strength with the presence of gas hydrates. Parameters β and μ can be used to account for the effect of S_H on HBS response (i.e. for a given hydrate morphology), and the parameter α can be used to model the effect of pore habit (i.e. for a given S_H). The parameter μ also controls the rate of mechanical damage. It was considered that the rate of mechanical damage increases with S_H, and it was also assumed that for the cementing morphology the rate of damage is higher than the pore-filling one. Generally, these parameters cannot be directly determined from experiments, and a number of tests (ideally three or more) are necessary to estimate them indirectly. An additional issue associated with the selection of model parameters for HBS is that the available data base is quite limited (at least when compared to the information existent for other types of soils and rocks). It is anticipated that as more experimental evidence become available and more insight on the behavior of HBS is gained, a better estimation of model parameters could be conducted.

2. CASE STUDY

To investigate the mechanical behavior of natural gas-hydrate-bearing sediments, several core samples were extracted from the Eastern Nankai Trough by Yoneda et al (2015). Two different core handling methods were adopted in this study, as follows:"LN2 core" and "CH4 purge LN2 core". It should be noted that both methods require the core samples to be depressurized at atmospheric pressure for a short period of time, which might cause hydrate dissociation, thus causing disruptions on the mechanical behavior of the sample.

Core N^o 7 (i.e. LN2 core method) and N^o 9 (i.e. CH_4 purge LN_2 core method), with hydrate saturation around 38% and 79%, respectively, were tested under triaxial drained condition. According to the mentioned reference, the possible in-situ hydrate saturation is in the range 65-90% for Core No. 7, while after handling, hydrate saturation dropped to 38% at test condition. Moreover, many fractures and cracks was observed in the CT image which means that the soil structure was affected by the handling method. For Core No. 9, the in-situ hydrate saturation is in the range of 70-95%, hydrate saturation at test condition is 79%. And no fractures and cracks were observed, which imply that when Core No.9 was tested, it was very close to in-situ condition. Based on the fact that Core No 7 and Core No.9 initial properties at test condition were very different, we modeled each test independently and parameter fitting was adopted to obtain the results. Table 1 lists the main soil index properties, alongside with the more relevant in-situ and testing conditions related to these samples and experiments.

Table 1. In situ conditions, soil index properties, and testing conditions

Test name	Host type	Over burden (m)	Effective confining pressure (MPa)	Test condition	Water Content (%)	Porosity	Hydrate saturation S_H (%)
No.7	Silty sand	279.3	1.5	CD	26.4	44.1	38
No.9	Silty sand	294.2	1.5	CD	22.7	39.4	79

Figure 1 presents the experimental stress-strain behavior and volumetric response of the natural hydrate-bearing core samples discussed above (with symbols) together with the model results (with lines). As in other cases, the MCCM was initially adopted to reproduce the observed experimental behavior. It is noticeable that the Core N^o 9 (with higher S_H) exhibits a much higher peak strength and a more noticeable enhancement in stiffness and dilatancy than Core N^o 7 To model these different responses, it was considered the dependence of μ on hydrate concentration. Considering the high concentration of hydrate in Core N^o 9, it was assumed that this specimen has a higher damage rate on shearing than Core N^o 7, and therefore a higher μ was adopted. Note two considerations: i) a fix value of β=1.6 was adopted for all the simulations in this paper, and ii) α depends mainly in hydrate pore habit, even though that part of Core N^o 7 might have dissociated during the handling process, the pore habit is assumed to remain the same, thus a unique value of α=12 for Core N^o 7 and Core N^o 9 was adopted.

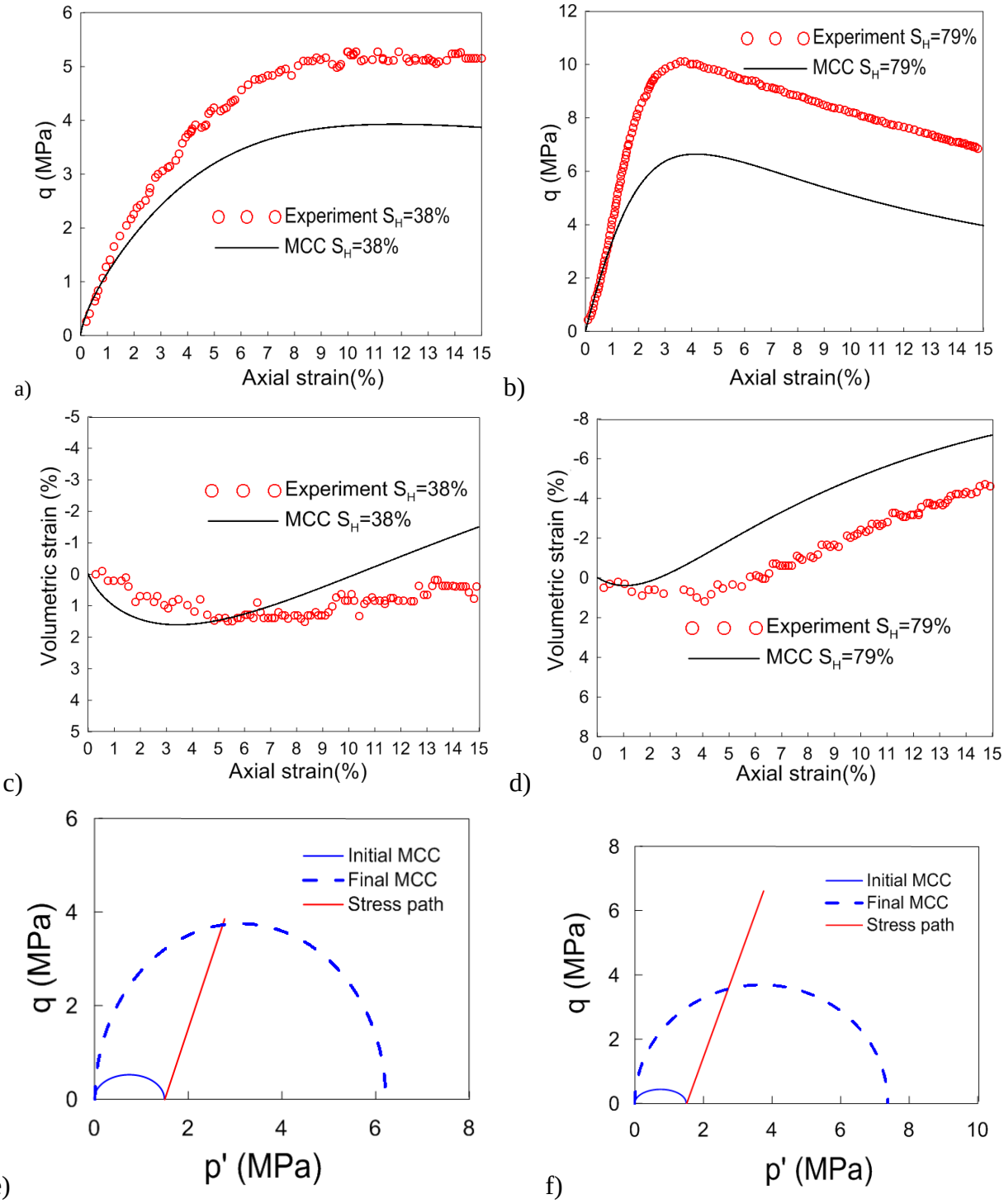

Figure 1. Modified Cam-Clay model results: a) stress strain relationship specimen S_H=38%; b) stress strain relationship specimen S_H =79%; c) volumetric response specimen S_H=38%; d) volumetric response specimen S_H =79%; e) stress path and yield surface evolution specimen S_H=38%; and f) stress path and yield surface evolution specimen S_H =79%. Experimental data after Yoneda et al. (2015).

It is clear that the MCCM performance is not very satisfactory in this case. Figure 1 a & b, shows that for both hydrate saturations the model under predicts the material strength. As for the volumetric behavior (i.e. Figures 1 c & d), the model slightly over-predict sediment dilation. This implies that any change in the parameters controlling the sediment strength and dilation enhancement (i.e. β, and μ), may improve the model prediction in terms of strength, but it will also increase the dilation and softening predictions, up to values that may be not acceptable. Figures 1 e & f shows the stress paths for the two tests with the corresponding initial and final MCC yield surfaces.

To improve the model performance, the HISS model flexibility was explored by changing the shape of the yield surface and plastic potential to obtain more satisfactory results. Figure 2 shows the initial HISS yield surface suggested for the two cores, together with the MCCM ones for comparisons purposes only. Figure 3 presents similar results to the ones introduced in Figure 1 for the MCCM. The model performance is evidently more satisfactory in this case, with better perditions in terms of sediment stiffness, strength and softening behavior (i.e. Figures 3 a & b) as well as in terms of volumetric behavior (i.e. Figures 3 c & d). Table 2 lists the parameters adopted in all the simulations. As shown the HISS-MH model provide enough flexibility to predict the mechanical behavior of two natural samples from Nankai Trough.

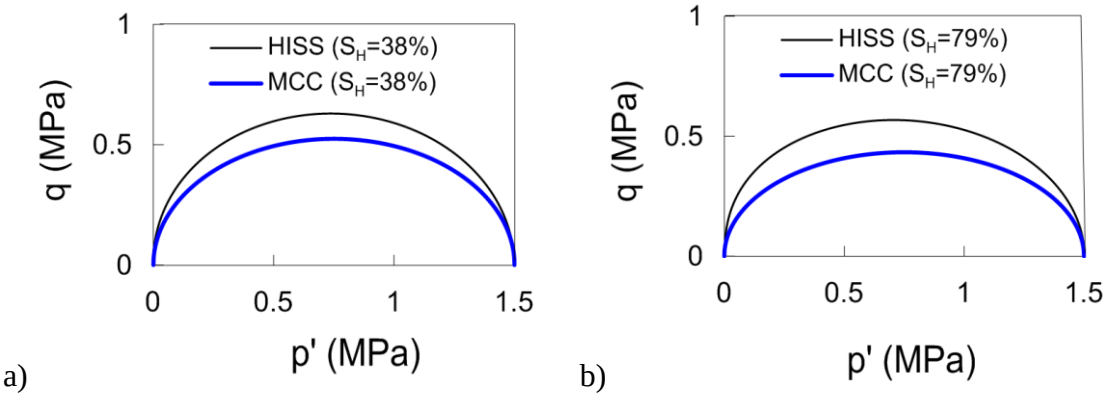

Figure 2. Initial yield surfaces adopted for MCCM and HISS a) specimen S_H 38%; and b) specimen S_H 79%

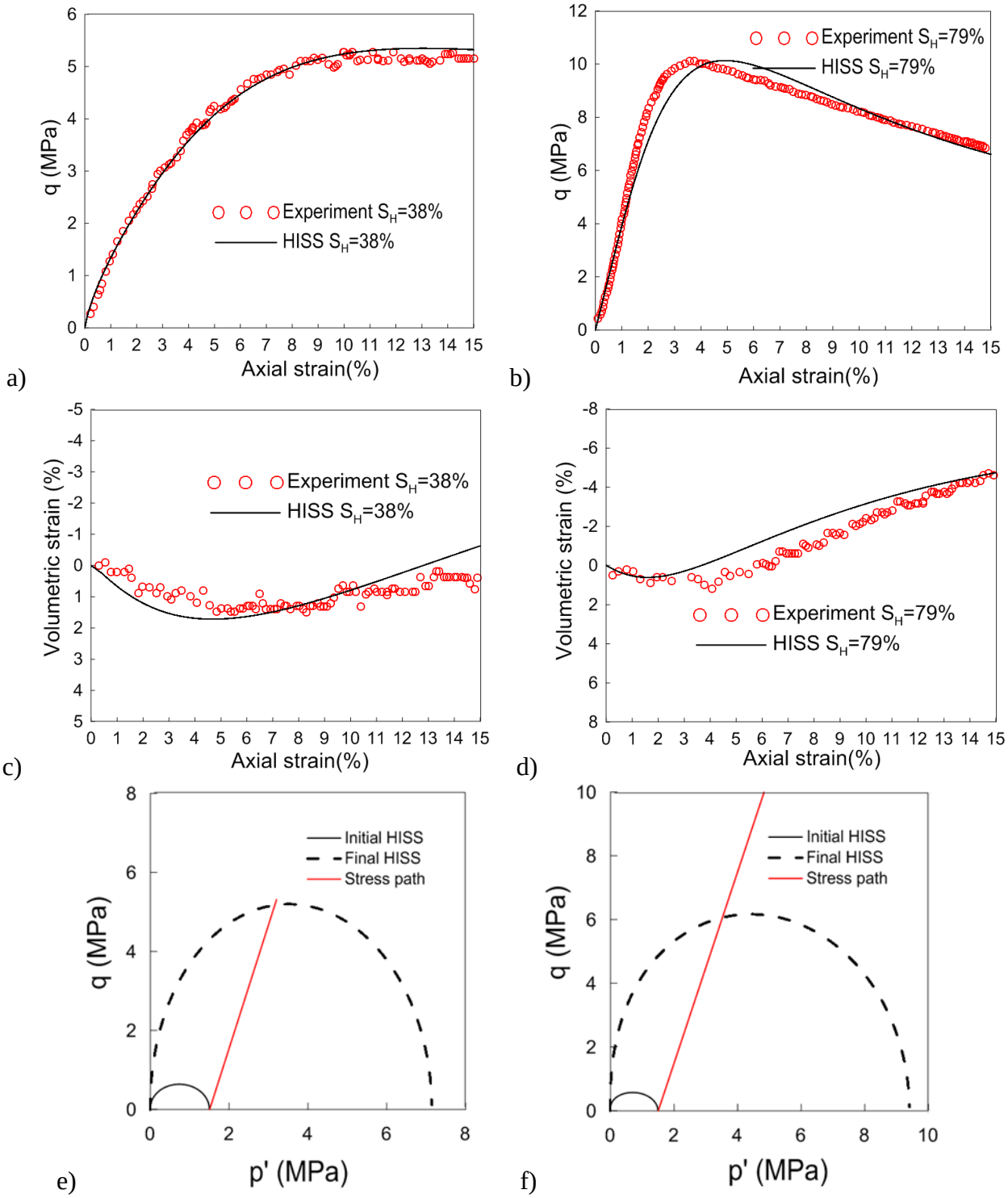

Figure 3. HISS model results: a) stress strain relationship specimen S_H=38%; b) stress strain relationship specimen S_H =79%; c) volumetric response specimen S_H=38%; d) volumetric response specimen S_H =79%; e) stress path and yield surface evolution specimen S_H=38%; and f) stress path and yield surface evolution specimen S_H =79%. Experimental data after Yoneda et al. (2015).

Table 2. Soil parameters adopted in the modeling of HBS specimens Case 2

S_H=38%

Properties	HISS	MCC
M	1.21	1.21
λ	0.13	0.13
κ	0.008	0.008
p_c (MPa)	12	12
n	0.95	1
a	3	3
γ	-0.15	-1/9
S_H	0.38	0.38
α	12	12
β	1.6	1.6
μ	1.0	1.0
η	2.7	2.7

S_H=79%

Properties	HISS	MCC
M	1.21	1.21
λ	0.13	0.13
κ	0.008	0.008
p_c (MPa)	12	12
n	0.95	1
a	3	3
γ	-0.15	-1/9
S_H	0.79	0.79
α	12	12
β	1.6	1.6
μ	3.5	3.5
η	28	28

3. FINAL REMARKS

This study presented the response of the HISS-HBS mechanical model when some of its ingredients are modified. In particular, this work focused on the effect of the yield surface on the capability of the model to describe the behavior of HBS under triaxial conditions. It was observed that the ‘single yield surface’ incorporated in the formulation of this constitutive equation provides more flexibility to reproduce the complex behavior of HBS observed in the experiments.

REFERENCES

Desai CS, Somasundaram S, Frantziskonis G. A hierarchical approach for constitutive modelling of geologic materials. International Journal for Numerical and Analytical Methods in Geomechanics. 1986;10(3):225-57.

Sanchez (2015). "THCM Coupled Model For Hydrate-Bearing Sediments: Data Analysis and Design of New Field Experiments (Marine and Permafrost Settings)". DOE Quarterly Research Performance Progress Report (Period ending 06/30/2015).

Uchida S, Soga K, Yamamoto K. Critical state soil constitutive model for methane hydrate soil. Journal of Geophysical Research: Solid Earth (1978–2012). 2012; 117(B3).

Yoneda, J, A Masui, Y Konno, Y Jin, K Egawa, M Kida, T Ito, J Nagao, and N Tenma, Mechanical properties of hydrate-bearing turbidite reservoir in the first gas production test site of the Eastern Nankai Trough. Marine and Petroleum Geology, 2015.

PRODUCTS

Publications – Presentations –Technical Sessions:

- Sánchez M. and Xuerui G. (2016). "Behavior of Hydrates Bearing Sediments". Keynote lecture 1st International Conference on Energy Geotechnics. Kiel, Germany. 29th to 31st Aug. 2016 (Accepted)
- Sánchez M., Falcão F., Mack M., Pereira JM, Narsilio G., Guimarães L. "Salient Comments from an Expert Panel on Energy Geotechnics". Environmental Geotechnics, Accepted.
- Gai X., and Sanchez M. "Mechanical Modeling of Gas Hydrate Bearing Sediments Using an Elasto-Plastic Framework". A revised version of the journal paper was submitted for a second review (Environmental Geotechnics).
- Sanchez M., Gai X., and Santamarina JC. "A Constitutive Mechanical Model for Gas Hydrate Bearing Sediments Incorporating Inelastic Mechanisms". A revised version of a journal paper was submitted for a re-review.
- "Session ID 12884: Hydrate bearing sediments: characterization, modeling, and thermal, hydrological, and geomechanical behavior". American Geophysical Union Fall 2016 Meeting, Dec. 2016, San Francisco, California. Conveners: Jeen-Shang Lin (Univ. of Pittsburgh), Yongkoo Seol (NETL, DOE), Marcelo Sanchez and Steve Phillips (The Univ. of Texas, Austin).
- "Mini-Symposium: Geomechanical characterization and modeling of hydrate bearing sediments". 1st International Conference on Energy Geotechnics. Kiel, Germany. 29th to 31st Aug. 2016. Organizers Marcelo Sanchez and Christian Deusner.

Website: Publications (for academic purposes only) and key presentations are included in: http://engineering.tamu.edu/civil/people/msanchez

Technologies or techniques: None at this point.

Inventions, patent applications, and/or licenses: None at this point.

Other products: None at this point.

PARTICIPANTS

Research Team: The current team is shown next.

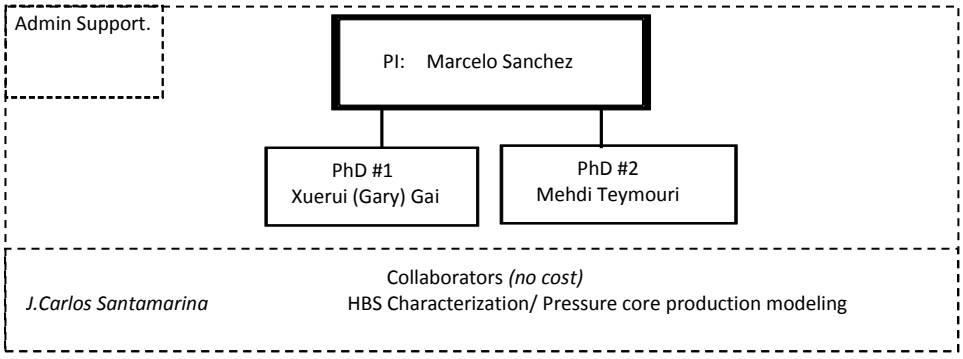

IMPACT

We can highlight the relevance of a computational platform extensively validated in a wide range of coupled thermo-hydro-chemo-mechanical coupled problems (CB_Hydrate).

CHANGES/PROBLEMS:

None so far.

SPECIAL REPORTING REQUIREMENTS:

Nothing to report

BUDGETARY INFORMATION:

							Budget Period 2							Budget Period 3			
Q3		Q4		Q1		Q2		Q3		Q4		Q1		Q2		Q3	
Enter date range		Enter date range		Enter date range		Enter date range		Enter date range		Enter date range		Enter date range		Enter date range		Enter date range	
04/01/14-06/30/14		07/01/14-9/30/14		10/1/14-12/31/2014		01/01/15-03/31/15		04/01/15-06/30/15		07/01/15-9/30/15		10/1/15-12/31/2015		01/01/16-03/31/16		04/01/16-06/30/16	
	Cumulative		Cumulative		Cumulative		Cumulative		Cumulative		Cumulative		Cumulative		Cumulative		Cumulative
Q3	Total	Q4	Total	Q1	Total	Q2	Total	Q3	Total	Q4	Total	Q1	Total	Q2	Total	Q3	Total
$ 40,500.00	$121,500.00	$ 92,180.00	$ 213,680.00	$ 27,600.00	$241,280.00	$ 27,600.00	$ 268,880.00	$ 27,600.00	$ 296,480.00	$ 92,080.00	$ 388,560.00	$ -	$388,560.00	$ -	$388,560.00	$ -	$ 388,560.00
$ 40,500.00	$121,500.00	$ 92,180.00	$ 213,680.00	$ 27,600.00	$241,280.00	$ 27,600.00	$ 268,880.00	$ 27,600.00	$ 296,480.00	$ 92,080.00	$ 388,560.00	$ -	$388,560.00	$ -	$388,560.00	$ -	$ 388,560.00
$ 11,223.00	$ 33,669.00	$ 11,223.00	$ 44,892.00	$ 11,223.00	$ 56,115.00	$ 11,223.00	$ 67,338.00	$ 11,223.00	$ 78,561.00	$ 11,223.00	$ 89,784.00	$ -	$ 89,784.00	$ -	$ 89,784.00	$ -	
$ 51,723.00	$155,169.00	$103,403.00	$ 258,572.00	$ 38,823.00	$297,395.00	$ 38,823.00	$ 336,218.00	$ 38,823.00	$ 375,041.00	$103,303.00	$ 388,560.00	$ -	$388,560.00	$ -	$378,732.88	$ -	$ 388,560.00
$ 33,827.48	$ 52,893.65	$ 51,567.77	$ 104,461.42	$ 80,352.17	$184,813.59	$ 24,626.18	$ 209,439.77	$ 19,260.19	$ 228,699.96	$ 29,858.73	$ 258,558.69	$ 13,074.57	$271,633.26	$ 23,720.88	$295,354.14	$ 10,225.86	$ 305,580.00
$ 10,170.37	$ 23,354.07	$ 58,205.62	$ 81,559.69	$ 92,208.79	$173,768.48	$ 31,359.66	$ 205,128.14	$ 19,260.19	$ 224,388.33	$ 29,812.17	$ 349,425.73	$ 4,088.61	$353,514.34	$ -	$ 83,378.74	$ -	$ 83,378.74
$ 20,743.19	$ 46,677.92	$ 29,262.19	$ 75,940.11	$ -	$ 75,940.11	$ -	$ 75,940.11	$ 8,833.66	$ 84,773.77	$ -	$ 84,773.77	$ -	$ 84,773.77	$ -	$ 84,773.77	$ -	$ 84,773.77
$ 30,913.56	$ 70,031.99	$ 87,467.81	$ 157,499.80	$ 92,208.79	$249,708.59	$ 31,359.66	$ 281,068.25	$ 28,093.85	$ 309,162.10	$ 29,812.17	$ 434,199.50	$ 8,985.96	$271,633.26	$ 23,360.37	$294,993.63	$ 10,225.86	$ 168,152.51
$ 20,809.44	$ 85,137.01	$ 15,935.19	$ 101,072.20	$(53,385.79)	$ 47,686.41	$ 38,823.00	$ 55,149.75	$ 10,729.15	$ 65,878.90	$ 73,490.83	$ (45,639.50)	$ (8,985.96)	$116,926.74	$ (23,360.37)	$ 83,739.25	$ (10,225.86)	$ 220,407.49
$ (23,657.11)	$ (29,539.58)	$ 6,637.85	$ (22,901.73)	$ 11,856.62	$ (11,045.11)	$ 6,733.48	$ (4,311.63)	$ -	$ (4,311.63)	$ 4,358.19	$ 46.56	$ 4,358.19	$ 4,404.75	$ 4,854.89	$ 9,259.64	$ 57,089.97	$ 57,089.97
$ (9,520.19)	$ (13,008.92)	$ (40,485.19)	$ (53,494.11)	$ 11,223.00	$ (42,271.11)	$ 6,733.48	$ (35,537.63)	$ 2,389.34	$ (33,148.29)	$ 11,223.00	$ (21,925.29)	$ -	$ (21,925.29)	$ -	$ (21,925.29)	$ (21,925.29)	$ (21,925.29)
$ (33,177.30)	$ (42,548.50)	$ (33,847.34)	$ (76,395.84)	$ 23,079.62	$ (53,316.22)	$ 13,466.96	$ (39,849.26)	$ 2,389.34	$ (37,459.92)	$ 15,581.19	$ (21,878.73)	$ 4,358.19	$ (17,520.54)	$ 4,854.89	$ (12,665.65)	$ 35,164.68	$ 22,499.03

National Energy Technology Laboratory

626 Cochrans Mill Road
P.O. Box 10940
Pittsburgh, PA 15236-0940

3610 Collins Ferry Road
P.O. Box 880
Morgantown, WV 26507-0880

13131 Dairy Ashford Road, Suite 225
Sugar Land, TX 77478

1450 Queen Avenue SW
Albany, OR 97321-2198

Arctic Energy Office
420 L Street, Suite 305
Anchorage, AK 99501

Visit the NETL website at:
www.netl.doe.gov

Customer Service Line:
1-800-553-7681